Calibration of the GNSS Signal Amplitudes in the Interference Pattern Technique for Altimetry

Jean-Christophe Kucwaj*, Miguel Angel Ribot‡, Georges Stienne*, Cyril Botteron‡,
Serge Reboul* , Jean-Bernard Choquel*, Pierre-André Farine‡ and Mohammed Benjelloun*
*Laboratoire d'Informatique, Signal et Image de la Côte d'Opale (LISIC), Univ Lille Nord de France,
F-59000 Lille, France, Université du Littoral Côte d'Opale (ULCO), F-62228 Calais, France
Email: kucwaj@lisic.univ-littoral.fr
‡Electronics and Signal Processing Laboratory (ESPLAB), École Polytechnique Fédérale de Lausanne (EPFL),
CH-2000 Neuchâtel, Switzerland. Email: miguel.ribotsanfelix@epfl.ch

***Abstract*—Global Navigation Satellite Systems signals can be used in bi-static radar systems in order to get altimetric measurements. With a single classic GNSS ground-based receiver processing the combination of the signals coming directly and after one reflection to the receiving antennas, the Interference Pattern Technique allows the computation of the height of the reflecting surface. In this case, the observed parameter is the Signal to Noise Ratio of the received composite signal, which oscillates at a frequency proportional to this height. However, the signal recordings are generally very long since the accuracy of the SNR frequency estimation is proportional to the variation of the satellite elevation during the observation interval. In this article, we propose a calibration technique that allows reducing the observation duration while keeping a centimeter accuracy performance. The proposed technique is tested on both synthetic and real data.**

I. Introduction

Since the first use of Global Navigation Satellite Systems (GNSS) signals for measuring the height of the oceans [1], GNSS-Reflectometry (GNSS-R) has become a well-established technique for Earth observation. Several applications have been studied, including the characterization of sea surface roughness [2], salinity [3] and temperature [4]; soil moisture estimation [5] and snow depth retrieval [6]. These applications are especially useful for coastal or wet area monitoring, or for avalanche prediction. In these local cases, ground-based or low-altitude airborne reflectometers are favored over spaceborne ones in order to get smaller antenna glistening zones and higher precision in the reflecting surface parameters estimation. Some of the advantages of using GNSS signals as signals of opportunity for bi-static radar measurements include the precision, the stability and the low sensibility of these signals to atmospheric perturbations, the global covering of the existing constellations over time and space, as well as the availability of several reflection observations at the same time.

Several approaches have been proposed for ground-based altimetric measurements using GNSS signals. The interferometry method firstly proposed for spaceborne application [1] has been more recently tested with antennas located on a bridge [7]. In this technique, the direct and reflected signals are correlated so the correlation peak delay reflects the range delay. However, directional GNSS antennas have to be used in order to observe a single satellite signal, preventing merging the observations of several footprints located at different heights. A second technique relies on phase ranging techniques: the phase delay between the direct and the reflected signals can be used to determine the vertical height of the reflecting surface [8]. However, phase ranging requires either an ambiguity resolution, which usually relies on multiple differences approaches (e.g. using several receivers), or long signal recording [9]. A third technique, named Interference Pattern Technique (IPT), relies on modeling the signal to noise ratio (SNR) oscillations in the composite direct plus reflected signal with the reflecting surface height [10]. These oscillations are indeed directly related to the cosine of the phase difference between both signals, thus to the path difference, and to the satellite elevation angle. The knowledge of these two parameters allows computing the reflecting surface height. However, long recording durations are generally needed for the IPT as well.

In this article, we propose to use a calibration technique that allows reducing the measurement duration in the IPT. It consists in moving vertically the receiving antennas in order to obtain fast SNR values of the minimum and maximum, so the observed oscillations for a constant height can be calibrated. Afterwards, the SNR frequency of oscillation, directly related to the distance to the reflecting surface, can then be estimated on a fraction of one period. We also propose an original experimental framework using two antennas, both receiving the signal coming directly from the GNSS satellite in order to precisely know the full system geometry and to assess the height estimation.

The paper is organized as follows. After this introduction, we state the height retrieval problem using the IPT approach in the second section. The third section is dedicated to the proposed techniques, including the calibration of the SNR, the SNR oscillations frequency estimator and the proposed experimental framework. The fourth section presents the results obtained on both synthetic and real data. The last section concludes the paper.

II. Problem statement

The geometry of a ground-based GNSS altimeter is shown on Figure 1. In this case, the Earth curvature can be ignored. In Figure 1, θ^s_{el} represents the elevation angle of the satellite, Δx^s is the horizontal distance between the antennas and the specular reflection point. h is the common height of the two antennas used for sensing the direct and reflected signals, respectively in right hand circular polarization (RHCP) and left hand circular polarization (LHCP). Multiple satellite signals can be used, depending on the location of the associated

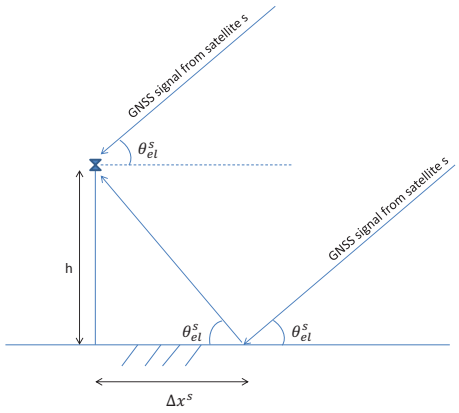

Fig. 1. System geometry in the case of a ground-based receiver.

specular point on the observed surface.The direct and reflected signals coming from a GPS-L1 satellite s can be modelled as

$$S^s_D(t) = A^s_D \cos\left(2\pi f^s_D t + \phi^s_D\right) d^s_D(t)\, CA^s\left(t - \tau^s_D\right) + \nu^s_D(t) \quad (1)$$

$$S^s_R(t) = A^s_R \cos\left(2\pi f^s_R t + \phi^s_D + \phi^s_R\right) d^s_R(t)\, CA^s\left(t - \tau^s_R\right) + \nu^s_R(t) \quad (2)$$

where A^s_D and A^s_R are the amplitudes of the direct and reflected signals, f^s_D and f^s_R their respective carrier frequencies, ϕ^s_D the carrier phase of the direct signal and ϕ^s_R is the phase delay between the direct and the reflected signals. τ^s_D and τ^s_R are the code delays of the signals and CA^s is the Coarse/Acquisition code of the signal. $d^s_D(t)$ and $d^s_R(t)$ represent the data messages. $\nu^s_D(t)$ and $\nu^s_R(t)$ are assumed to be additive white Gaussian noises (AWGN). When the direct and reflected signals are combined at the receiver, the expression of the processed signal can be expressed as

$$\begin{aligned} S^s_G(t) = {} & A^s_D \cos\left(2\pi f^s_D t + \phi^s_D\right) d^s_D(t)\, CA^s\left(t - \tau^s_D\right) + \nu^s_D(t) \\ & + A^s_R \cos\left(2\pi f^s_D t + \phi^s_D + \phi^s_R\right) d^s_R(t)\, CA^s\left(t - \tau^s_D\right) + \nu^s_R(t) \end{aligned} \quad (3)$$

In the case of an static, ground-based receiver, the code delays and carrier frequencies can indeed be assumed to be the same for the direct and received sampled signals. It has been shown in [11] that

$$\phi^s_R = 4\pi \frac{f_{L1}}{c}\, h\, \sin(\theta^s_{el}) \quad (4)$$

where f_{L1} is the GPS-L1 carrier frequency and h is the height between the antennas and the reflecting surface. c is the signal propagation speed, namely the speed of light. As presented in [11], the sampled global signal $S^s_G[n]$ can be also expressed as

$$S^s_G[n] = A^s_G\, CA^s\left[nT^s - \tau^s_D\right] \cos\left(X - \phi^s_G\right) + \nu^s_G \quad (5)$$

with T_{chip} the code chip period and:

$$X = 2\pi f^s_D t + \phi^s_D \quad (6)$$

$$\phi^s_G = \arctan\left(\frac{A^s_R \sin(\phi^s_R)}{A^s_D + A^s_R \cos(\phi^s_R)}\right) \quad (7)$$

$$A^s_G = \sqrt{(A^s_D)^2 + (A^s_R)^2 + 2A^s_D A^s_R \cos(\phi^s_R)} \quad (8)$$

The carrier to noise ratio C/N_0 of a GNSS signal can be estimated after the demultiplexing and demodulation stages. The C/N_0 is proportional to the amplitude A^s_G of the received signals. Equation (8) links the amplitude to the cosine of the phase delay between the direct and reflected signal. Equation (4) shows that the phase delay varies proportionally to the sinus of the satellite elevation, with a frequency $4\pi\frac{f_{L1}}{c}h$. Consequently, the amplitude of the received signal will oscillate with a frequency proportional to the antenna height.

In order to be able to estimate the frequency of the amplitude oscillations, i.e. the frequency of $\cos(\phi^s_R)$, traditional IPT approaches usually make use of at least one period of the signal. For a given initial elevation $\theta^s_{el^0}$, the satellite elevation variation $\Delta\theta^s_{el}$ corresponding to one period of $\cos(\phi^s_R)$ can be defined, according to equation (4), by:

$$\frac{c}{2f_{L1}h} - \sqrt{2 - 2\,\cos(\Delta\theta^s_{el})}\, \cos\left(\theta^s_{el^0} + \frac{\Delta\theta^s_{el}}{2}\right) = 0 \quad (9)$$

The results obtained from this equation are displayed Figure

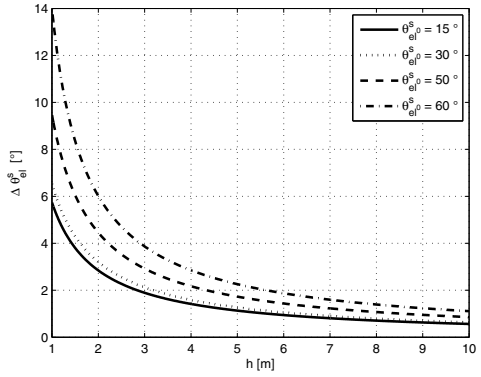

Fig. 2. Satellite elevation variations required for observing one period of oscillation in the measured signal amplitude.

2 for three different values of $\theta^s_{el^0}$. For example, for an antenna height of 2 m and for any initial elevation, one period of oscillation will be observed for a variation of elevation of at least 2.8°. For a mean satellite elevation speed of 5.10^{-3} °/s, this corresponds to 9 minutes and 20 seconds of signal observation (i.e. 560 seconds). In the next section, we firstly propose a calibration method for the evolution of A^s_G, which can then be modeled with the signal frequency as the single unknown parameter. We then build an estimator based on this calibration to provide a frequency estimate with no restriction on the observed duration of the signal, meaning a fraction of one period of the signal can be used.

III. Proposed approach

A. Calibration of the GNSS signal amplitudes

Equation (4) describes the phase ϕ^s_R as a function of both, the antenna height and the satellite elevation. From Equation (8), it is possible obtain the minimum ($A^s_{G,min}$) and maximum ($A^s_{G,max}$) values of A^s_G for $\cos(\phi^s_R)$ respectively equal to -1 and 1. We propose a calibration procedure based on fast variations of the antennas height to observe these minimum and maximum values during short signal observation times. In this case we have:

$$(A^s_{G,min})^2 = (A^s_D)^2 + (A^s_R)^2 - 2A^s_D A^s_R \quad (10)$$

$$(A^s_{G,max})^2 = (A^s_D)^2 + (A^s_R)^2 + 2A^s_D A^s_R \quad (11)$$

Then, by adding the two expressions, we obtain:

$$(A_D^s)^2 + (A_R^s)^2 = \frac{(A_{G,max}^s)^2 + (A_{G,min}^s)^2}{2} \quad (12)$$

$$2A_D^s A_R^s = \frac{(A_{G,max}^s)^2 - (A_{G,min}^s)^2}{2} \quad (13)$$

Thus, knowing $A_{G,min}^s$ and $A_{G,max}^s$, $\cos(\phi_R^s)$ becomes the only unknown parameter in Equation (8).
In order to obtain $A_{G,min}^s$ and $A_{G,max}^s$, we want to observe a whole 2π-period of the phase ϕ_R^s. According to Equation (4), the corresponding value of the antenna height variation, dh, is given by:

$$dh = \frac{c}{2\ f_{L1} \sin(\theta_{el}^s)} \quad (14)$$

We show on Table I dh as a function of the satellite elevation, θ_{el}^s. By assuming that the LHCP component of the reflected signal is dramatically attenuated for elevations below 10° [12], we can consider a variation of 50 cm as sufficient to estimate $A_{G,max}^s$ and $A_{G,min}^s$ for any of the usable satellite signals.

θ_{el}^s (°)	10	25	40	55	70	85
dh (cm)	55	23	15	12	10	10

TABLE I. ANTENNA HEIGHT VARIATIONS NECESSARY TO OBSERVE ONE PERIOD OF ϕ_R^s.

In the next section, we propose an estimator for the frequency of $\cos(\phi_R^s)$ assuming that $A_{G,max}^s$ and $A_{G,min}^s$ are known, i.e. an estimator of $4\pi\frac{f_{L1}}{c}h$.

B. Frequency estimation

For each satellite, the GNSS receiver provides noisy C/N_0 measurements from which we can obtain noisy A_G^s measurements [13]. Let us define $y^s[n]$ as the n^{th} measurement of A_G^s. Then, we have:

$$y^s[n] = \sqrt{(A_D^s)^2 + (A_R^s)^2 + 2\ A_D^s\ A_R^s\ \cos(\phi_R^s[n])} + \omega[n] \quad (15)$$

where $\omega[n]$ is zero-mean AWGN. According to Equation (4), we model $\phi_R^s[n]$ as a linear function of $\sin(\theta_{el}^s[n])$, with a constant slope β:

$$\phi_R^{s,model}[n] = \beta\ \sin(\theta_{el}^s[n]) \quad (16)$$

When the model corresponds to the true phase, we have:

$$h = \frac{\beta\ c}{4\pi\ f_{L1}} \quad (17)$$

Finally, with Equations (12) and (13), we can write:

$$\begin{cases} \cos(\phi_R^s[n]) = \frac{2y^s[n]^2 - (A_{G,max}^s)^2 - (A_{G,min}^s)^2}{(A_{G,max}^s)^2 - (A_{G,min}^s)^2} \\ \cos(\phi_R^{s,model}[n]) = \cos(\beta\ \sin(\theta_{el}^s[n])) \end{cases} \quad (18)$$

The satellite elevation can be obtained from the current GPS satellites ephemeris and from the estimated position of the receiver, both being provided by the GNSS receiver. $A_{G,max}^s$ and $A_{G,min}^s$ are obtained from the calibration process. We thus can estimate the β value that best suits the A_G^s observations using as follows:

$$\hat{\beta} = \underbrace{\text{argmin}}_{\beta} \left\{ \sum_{n=1}^{N} \left(\cos(\phi_R^s[n]) - \cos(\phi_R^{s,model}[n]) \right)^2 \right\} \quad (19)$$

This estimation is highly non-linear due to the presence of sine and cosine functions within the expression of $\cos(\phi_R^{s,model}[n])$. Thus, we can estimate β by using a brute force approach, i.e. by testing its possible values in a interval bounded by a minimum and a maximum expected height. The expected accuracy will obviously depend on the employed step of search of β and on the number of observations. The expected accuracy is also function of the relative satellite-receiver geometry. The influence of the satellite elevation and of the satellite elevation variation rate will be evaluated in the synthetic data experiments, described in Section IV-A.

C. Experimental framework

In order to accurately assess the proposed method on real data, we developed an original experimental setup in which we aim to measure the height difference between two antennas, one of them simulating the specular point. This height can be estimated using the calibrated IPT. The advantage of the proposed setup is that the whole system geometry, including the height to estimate, are precisely known. The relation between the height difference of the two antennas and the frequency of the variations of the GNSS signal power has to be redefined for this special case. We show the geometry of

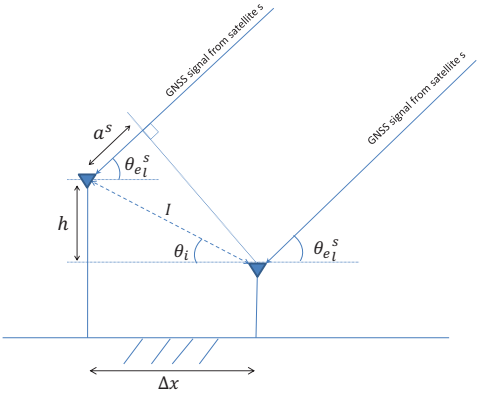

Fig. 3. System geometry for the real data experiments.

the experimental framework Figure 3. For a height h between the two antennas, and for the satellites in the vertical plane containing the two antennas, we have:

$$h = I\ \sin(\theta_i) \quad (20)$$

$$a^s = I\ \cos(\theta_i + \theta_{el}^s) \quad (21)$$

where I is the distance between the two antennas, a^s is the path difference between the two GNSS signals and θ_i is the angle between the two antennas and the ground. This method is only valid for satellites with an azimuth close to the direction of the experimental setup. The direction of the experimental

setup is defined by the vector that connects the two antennas and is constant during the experiment. We can thus write:

$$\begin{aligned}\frac{a^s}{h} &= \frac{\cos(\theta_i+\theta^s_{el})}{\sin\ \theta_i} = \frac{\cos\ \theta^s_{el}}{\tan\ \theta_i} - \sin\ \theta^s_{el} \\ &= \sqrt{\frac{1}{\tan^2\ \theta_i}+1}\sin\left(\theta^s_{el}+\arctan^*\left(\frac{1}{\tan\ \theta_i}-1\right)\right) \\ &= K\sin(\theta^s_{el}+K_0) \qquad (22)\end{aligned}$$

with:

$$K = \sqrt{\frac{1}{\tan^2\ \theta_i}+1} \qquad (23)$$

$$K_0 = \arctan^*\left(\frac{1}{\tan\ \theta_i}-1\right) \qquad (24)$$

where $\arctan^*()$ is the four-quadrant inverse tangent. Finally, it follows that

$$a^s = h\ K\ \sin(\theta^s_{el}+K_0) \qquad (25)$$

and the phase ϕ^s_R can be written as

$$\phi^s_R = \frac{2\pi}{\lambda}a^s = \frac{2\pi}{c}f_{L1}a^s = \frac{2\pi}{c}f_{L1}h\ K\ \sin(\theta^s_{el}+K_0) \qquad (26)$$

ϕ^s_R evolves linearly as a function of $\sin(\theta^s_{el}+K_0)$. The slope of this evolution is $\frac{2\pi}{c}f_{L1}h\ K$, which it is also the frequency of the cosine variation of the SNR as defined in Equation (15).

IV. Experimentation

A. Synthetic data

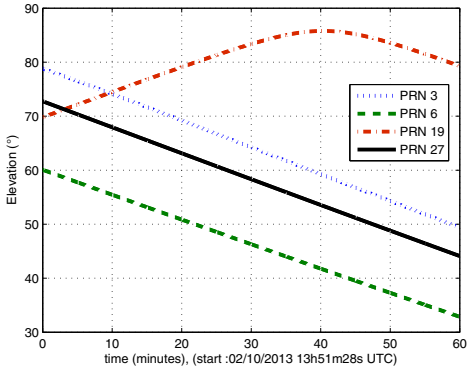

Fig. 4. Elevations of the satellites in view in Calais on the 2nd of October, 2013.

The aim of the experiments using synthetic data is to measure the expected accuracy of the proposed technique in the true reflectometry case (Figure 1). We generated these synthetic data for a constant direct signal C/N_0 of 50 dB-Hz. The power ratio between the reflected and the direct signals A_r^2/A_d^2 was set to 70% for all satellites. In LHCP, this corresponds to a minimum reflection coefficient on a smooth water surface with an elevation angle higher than 15° [12]. The height difference h between the two receiving antennas was set to 2 m. h was searched with a step of 1 mm in a bounded interval.

Figure 4 shows the variations of 4 satellite elevation angles over 60 minutes for a real scenario observed in Calais the 2nd of October 2013. Figure 5 shows the corresponding elevation variation rates. The observations were taken once per second. In Figure 6 we present the root mean square error (RMSE) of the estimated height, computed each minute after 600 seconds of observation. According to section II, this duration of observation corresponds to the minimum time required to observe one complete oscillation period of the signal for an initial satellite elevation close to 50°. One can observe two effects related to the satellite elevation. First, for satellite 19, low elevation variation rates show an important increase of the RMSE, which reaches values of more than one meter. Second, for satellites 3 and 27, and compared to the case of satellite 6, high elevation values imply centimeter levels of additional errors. These problems are linked to the presence of the elevation in Equation 18. We report in Table II the RMSE of the estimated height for satellite 6 at 14h01 as a function of the signal C/N_0 and of the number of considered samples. These results correspond to an optimal satellite-receiver geometry as defined previously in Figure 6. In this context, a complete oscillation period of the measured signal amplitude is observed after approximately 800 s. The results show the consistency of the estimator: as expected, longer observation times and higher C/N_0 result in lower RMSE. Centimeter accuracy can be expected for signals with a C/N_0 above 45 dB-Hz, even for an observation of 400 s.

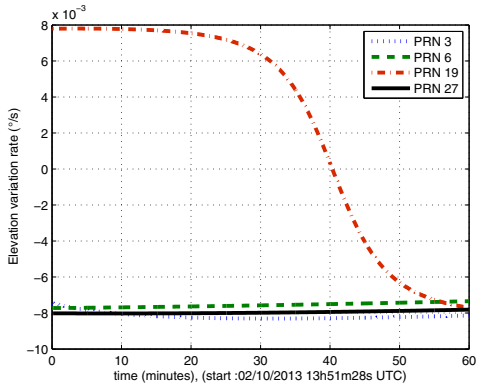

Fig. 5. Elevation variation rates of the satellites in view in Calais on the 2nd of October, 2013.

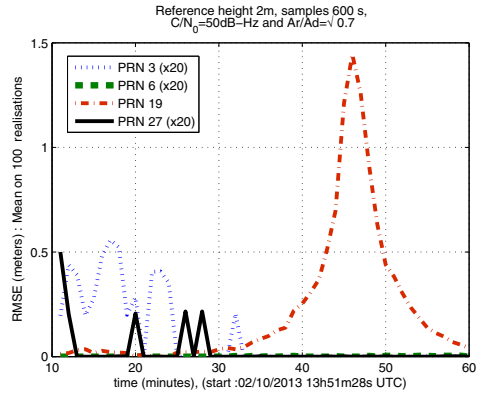

Fig. 6. Estimated height RMSE using synthetic signals for satellite behaviours presented Figures 4 and 5.

Samples (at 1 Hz) \ C/N_0	50 dB-Hz	45 dB-Hz	30 dB-Hz
800	0.0001	0.0129	0.0637
400	0.0228	0.0431	0.1507
200	0.0969	0.1377	0.4787

TABLE II. RMSE OF THE ESTIMATED HEIGHT, IN METERS, FOR THE SATELLITE PRN 6 THE 2ND OF OCTOBER 2013 AT 14H01M UTC (MEAN ON 1000 REALISATIONS, $h = 2\ m$, $A_r/A_d = \sqrt{0.7}$).

B. Real data

For the real data experiment, we implemented the experimental framework proposed in Section III-C. Figure 7 shows the vehicle carrying the whole altimeter on the left and the telescopic mast used for the calibration process on the right. The first direct antenna was located at the top of a mast that can go up to a height of 10 m. The second direct antenna was fixed on the roof of the car. The direction of the vehicle defines the direction in which satellites can be used as emitter for our bi-static radar. The horizontal distance between the two antennas was set to $\Delta x = 1.92$ m. Knowing the height difference between the antennas, one can derive the value of θ_i and assume that the whole system geometry is precisely known. The aim of the experiment is to obtain the height difference between the two antennas from the cosine evolution of the observed GNSS signal amplitudes.
Figure 8 shows an example of C/N_0 evolution as a function of $\sin(\theta_{el} + K_0)$. In this figure, we differentiate two stages: the calibration step, in which the telescopic mast is used to change the antennas height difference, and the observation step, in which the antennas height difference is kept constant. In the experimental setup, the calibration is realized at first with an antenna height variation of $dh = 0.5$ m. In accordance with the Sections III-A and III-C, we chose to exclude all the satellites with a low elevation and/or an azimuth distant from the direction of the vehicle. The height difference is estimated during the observation step using one half-period of the signal amplitude oscillation.

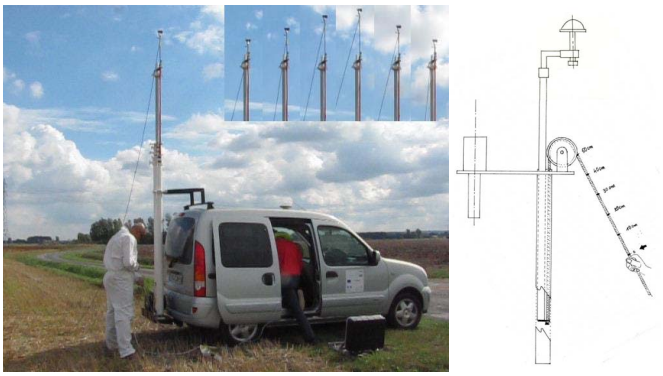

Fig. 7. Experimental setup: the vehicle and its telescopic mast.

We present in Tables III and IV the estimated height differences obtained from experiments realized on the 25th of September 2013 and on the 2nd of October 2013 in Calais. Figures 9 and 10 show the constellation of visible satellites and the direction of the experimental setup during each experimentation (skyplot). This direction was changed in order to have a maximum number of satellites in view.

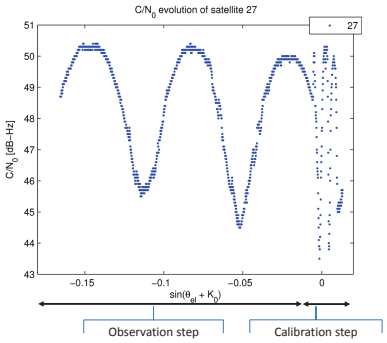

Fig. 8. Evolution of C/N_0 for one satellite.

On the 25th of September 2013 experiment, the reference height difference was fixed at $h = 2.15$ m and the azimuths of satellites 3, 6, 16, 19 and 27 reach the direction of the experimental setup. We can see in Figure 9 that satellite 19 has an elevation lower than $15°$ and that satellite 16 reaches an azimuth angle close to the direction of the vehicle only at the beginning of the experiment, i.e. during the step of calibration. Satellites 3, 6 and 27 were considered usable.We report in Table III the height estimated using the proposed method. The results show differences with the reference height inferior to 2 cm. On the 2nd of October 2013 experiment, the reference height difference was fixed at $h = 1.70$ m and satellites 3, 6 and 27 were at approximately $15°$ of azimuth angle with respect to the direction of the experimental setup. The estimated height obtained for these satellites presents, as shown in Table IV, differences with the reference height between 5 cm and 10 cm.

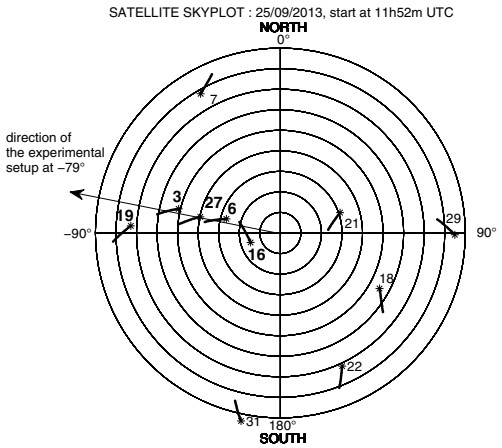

Fig. 9. Trajectories of the satellites in view during the measurements, the 25th of September 2013. Star symbols depict the end of the trajectories.

With the results reported in Tables III and IV, we can conclude that centimeter accuracy was reached for the visible satellites close to the direction of the experimental setup. It also appears that the considered satellites that were the more distant from the setup direction provided the worst results (satellites observed the 2nd of October). This observation only shows the limitation of the proposed experimental setup and would not

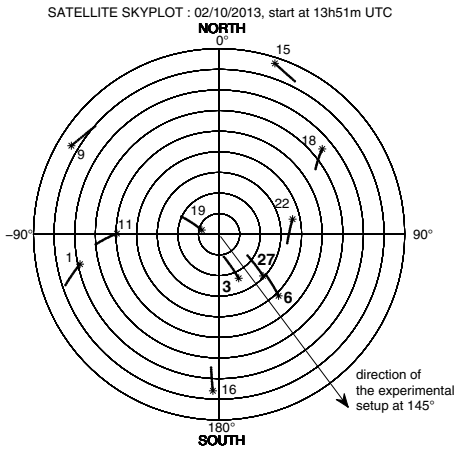

Fig. 10. Trajectories of the satellites in view during the measurements, the 2nd of October 2013. Star symbols depict the end of the trajectories.

Satellite number	Estimated height (m)	Elevation average (°)	Azimuth average (°)
3	2.1464	34.60	-78.80
6	2.1541	58.21	-78.32
27	2.1348	47.82	-81.54

TABLE III. ESTIMATED HEIGHT THE 25TH OF SEPTEMBER 2013 AT 11H52M UTC. REFERENCE HEIGHT: $h = 2.15\ m$. DIRECTION OF THE EXPERIMENTAL SETUP: $-79\ °$.

Satellite number	Estimated height (m)	Average Elevation (°)	Average Azimuth (°)
3	1.7566	72.25	159.61
6	1.8042	53.74	133.69
27	1.7805	66.14	130.60

TABLE IV. ESTIMATED HEIGHT THE 2ND OF OCTOBER 2013 AT 13H51M UTC. REFERENCE HEIGHT: $h = 1.7\ m$. DIRECTION OF THE EXPERIMENTAL SETUP: $145\ °$.

affect the results in a real reflectometry experiment.

V. CONCLUSION

This article proposes an original interference pattern for the estimation of the height of a reflecting surface, using a single GNSS receiver. The processed signal is the combination of a direct GNSS signal with the same signal received after reflection on the surface. We have shown that the amplitude of the resulting signal oscillates with a frequency proportional to the height of the surface. The proposed estimator of this frequency is based on two steps: a step of calibration and step of estimation. The calibration provides the minimum and maximum values of the signal amplitude to the estimator. This allows modeling the amplitude of the signal with a single unknown parameter: the height of the reflecting surface. The aim is to reduce the observation time needed to produce a precise altimetric measurement.

In this work, we have also proposed an experimental framework that uses two direct signals in order to allow the evaluation of the precision of altimetric measurements with real data. The advantage of this framework is that we have full knowledge of the system geometry. Using synthetic data we have shown that the proposed height estimate is consistent with the number of observations and with the power of the GNSS signal. We have also shown that the expected accuracy is a function of both the satellite elevation and the satellite elevation variation rate and that, by using the proposed method, less than one period of the signal amplitude oscillation is required in order to estimate the height. Finally, the results obtained using real data were consistent with the ones obtained using the synthetic signal and showed that the proposed technique can provide centimeter accuracy.

ACKNOWLEDGMENTS

This work has been partially supported by the Syndicat Mixte de la Côte d'Opale de la région Nord pas de Calais and by the Swiss National Science Foundation (SNSF) under grant no. 200020-153052.

REFERENCES

[1] M. Martin-Neira, "A passive reflectometry and interferometry system (PARIS): application to ocean altimetry," *ESA Journal*, vol. 17, no. 4, pp. 331–355, 1993.

[2] J. Garrison, A. Komjathy, V. Zavorotny, and S. Katzberg, "Wind speed measurement using forward scattered GPS signals," *IEEE Transactions on Geoscience and Remote Sensing*, vol. 40, no. 1, pp. 50–65, 2002.

[3] R. Sabia, M. Caparrini, and G. Ruffini, "Potential synergetic use of GNSS-R signals to improve the sea-state correction in the sea surface salinity estimation: Application to the SMOS mission," *IEEE Transactions on Geoscience and Remote Sensing*, vol. 45, no. 7, pp. 2088–2097, 2007.

[4] A. Camps, X. Bosch-Lluis, I. Ramos-Perez, J. F. Marchán-Hernández, N. Rodríguez, E. Valencia, J. M. Tarongi, A. Aguasca, and R. Acevo, "New passive instruments developed for ocean monitoring at the remote sensing lab Universitat Politècnica de Catalunya," *Sensors*, vol. 9, no. 12, pp. 10 171–10 189, 2009.

[5] D. Masters, V. Zavorotny, S. Katzberg, and W. Emery, "GPS signal scattering from land for moisture content determination," in *IEEE International Geoscience and Remote Sensing Symposium (IGARSS)*, vol. 7, 2000, pp. 3090–3092.

[6] C. Botteron, N. Dawes, J. Leclère, J. Skaloud, S. Weijs, and P.-A. Farine, "Soil Moisture & Snow Properties Determination with GNSS in Alpine Environments: Challenges, Status, and Perspectives," *Remote Sensing*, vol. 5, no. 7, pp. 3516–3543, 2013.

[7] A. Rius, O. Nogués-Correig, S. Ribó, E. Cardellach, S. Oliveras, E. Valencia, H. Park, J. Tarongí, A. Camps, H. van der Marel *et al.*, "Altimetry with GNSS-R interferometry: first proof of concept experiment," *GPS solutions*, vol. 16, no. 2, pp. 231–241, 2012.

[8] R. Treuhaft, S. Lowe, C. Zuffada, and Y. Chao, "2-cm GPS altimetry over Crater Lake," *Geophysical Research Letters*, vol. 28, no. 23, pp. 4343–4346, 2001.

[9] M. Semmling, G. Beyerle, R. Stosius, G. Dick, J. Wickert, F. Fabra, E. Cardellach, S. Ribó, A. Rius, A. Helm *et al.*, "Detection of Arctic ocean tides using interferometric GNSS-R signals," *Geophysical Research Letters*, vol. 38, no. 4, 2011.

[10] K. Larson, J. Löfgren, and R. Haas, "Coastal sea level measurements using a single geodetic GPS receiver," *Advances in Space Research*, vol. 51, no. 8, pp. 1301–1310, 2013.

[11] K. M. Larson, E. E. Small, E. Gutmann, A. Bilich, P. Axelrad, and J. Braun, "Using GPS multipath to measure soil moisture fluctuations: initial results," *GPS Solutions*, vol. 12, no. 3, pp. 173–177, 2007.

[12] V. Zavorotny and A. Voronovich, "Scattering of GPS signals from the ocean with wind remote sensing application," *IEEE Transactions on Geoscience and Remote Sensing*, vol. 38, no. 2, pp. 951–964, 2000.

[13] A. Bourkane, S. Reboul, M. Azmani, J.-B. Choquel, B. Amami, and M. Benjelloun, "C/N0 Inversion for soil moisture estimation using land-reflected bi-static radar measurements," in *Workshop on Reflectometry Using GNSS and Other Signals of Opportunity (GNSS+R)*, 2012, pp. 1–5.